

# Dry deposition of pollutant and marker particles onto live mouse airway surfaces enhances monitoring of individual particle mucociliary transit behaviour

Martin Donnelley,<sup>a,b,c,\*</sup> Kaye S. Morgan,<sup>d</sup> Karen K. W. Siu<sup>d,e,f</sup> and David W. Parsons<sup>a,b,c,g</sup>

<sup>a</sup>Respiratory and Sleep Medicine, Women's and Children's Health Network, North Adelaide, SA 5006, Australia, <sup>b</sup>School of Paediatrics and Reproductive Health, University of Adelaide, SA 5000, Australia, <sup>c</sup>Centre for Stem Cell Research, University of Adelaide, SA 5000, Australia, <sup>d</sup>School of Physics, Monash University, Clayton, Vic 3800, Australia, <sup>e</sup>Monash Biomedical Imaging, Monash University, Clayton, Vic 3800, Australia, <sup>f</sup>Australian Synchrotron, Clayton, Vic 3800, Australia, and <sup>g</sup>Women's and Children's Health Research Institute, North Adelaide, SA 5006, Australia.  
E-mail: martin.donnelley@adelaide.edu.au

Particles suspended in the air are inhaled during normal respiration and unless cleared by airway defences, such as the mucociliary transit (MCT) system, they can remain and affect lung and airway health. Synchrotron phase-contrast X-ray imaging (PCXI) methods have been developed to non-invasively monitor the behaviour of individual particles in live mouse airways and in previous studies the MCT behaviour of particles and fibres in the airways of live mice after deposition in a saline carrier fluid have been examined. In this study a range of common respirable pollutant particles (lead dust, quarry dust and fibreglass fibres) as well as marker particles (hollow glass micro-spheres) were delivered into the trachea of live mice using a dry powder insufflator to more accurately mimic normal environmental particulate exposure and deposition *via* inhalation. The behaviour of the particles once delivered onto the airway surface was tracked over a five minute period *via* PCXI. All particles were visible after deposition. Fibreglass fibres remained stationary throughout while all other particle types transited the tracheal surface throughout the imaging period. In all cases the majority of the particle deposition and any airway surface activity was located close to the dorsal tracheal wall. Both the individual and bulk motions of the glass bead marker particles were visible and their behaviour enabled otherwise hidden MCT patterns to be revealed. This study verified the value of PCXI for examining the post-deposition particulate MCT behaviour in the mouse trachea and highlighted that MCT is not a uniform process as suggested by radiolabel studies. It also directly revealed the advantages of dry particle delivery for establishing adequate particulate presence for visualizing MCT behaviour. The MCT behaviour and rate seen after dry particle delivery was different from that in previous carrier-fluid studies. It is proposed that dry particle delivery is essential for producing environmentally realistic particle deposition and studying how living airway surfaces handle different types of inhaled particles by MCT processes.

## 1. Introduction and objectives

Airborne pollutants suspended in the air in liquid, gaseous or solid forms are a considerable health concern (Happo *et al.*, 2010). We have previously described new techniques for

imaging solid particulates and fibres such as quarry dust, fibreglass, asbestos and lead in the nasal airways (Donnelley *et al.*, 2009) and trachea (Donnelley, Siu *et al.*, 2010) of live anaesthetized mice. These pollutants have the potential to produce acute health effects and can impact on respiratory

diseases such as cystic fibrosis (CF), asthma, bronchitis and emphysema as well as respiratory allergies and heart disease (O'Connor *et al.*, 2008). For example, CF patients living in regions with high-particulate-matter air pollution, such as in metropolitan areas, exhibit decreased lung function as well as an increased risk of pulmonary exacerbations (Goss *et al.*, 2004). The manner in which particulates deposit onto the airway surface and their behaviour after deposition remain poorly understood, but are likely to influence or predict key aspects of their subsequent pathophysiology.

Inhaled particles are cleared from the airways by mucociliary transit (MCT) and the effectiveness of the MCT system is a diagnostic indicator of airway health. To determine the efficacy of genetic (Stocker *et al.*, 2009; Limberis *et al.*, 2002) and other potential therapies for CF airway disease in animal models and potentially in humans we have developed novel MCT monitoring methods, based on measuring the transit rate and behaviour of individual deposited particles, that can be used *in vivo* in mice (Donnelley *et al.*, 2009; Donnelley, Siu *et al.*, 2010). By comparison, conventional methods for measuring bulk particle clearance from the airways (Grubb *et al.*, 2004; Donaldson *et al.*, 2007; Livraghi & Randell, 2007; Hua *et al.*, 2010) are unable to non-invasively detect and track the motion of *individual* pollutant particles in real time or with high resolution. Direct non-invasive visualization of the behaviour of deposited particles in animal-model airways will further improve our understanding of the MCT of individual particles that could contribute to a better understanding of airway health and disease.

Phase-contrast X-ray imaging (PCXI) is particularly useful for producing enhanced soft tissue contrast where the absorption differences are small, since it utilizes X-ray refraction in addition to conventional absorption. Provided the X-ray beam has sufficient spatial coherence and the sample-to-detector distance is sufficiently long (Snigirev *et al.*, 1995; Cloetens *et al.*, 1996; Wilkins *et al.*, 1996), tissue boundaries are enhanced by the phase changes induced by differences in their X-ray refractive indices. Our group has already shown the benefits of PCXI for non-invasive airspace imaging in small animals (Parsons *et al.*, 2008), for non-invasive particulate detection in live mouse airways (Donnelley *et al.*, 2009; Donnelley, Siu *et al.*, 2010; Siu *et al.*, 2008) and for the visualization of fluid dosing for gene therapy treatments in live mice (Donnelley *et al.*, 2011).

Our previous studies (Donnelley *et al.*, 2009; Donnelley, Siu *et al.*, 2010) delivered particulates in a 15  $\mu\text{l}$  to 50  $\mu\text{l}$  bolus of 0.9% saline carrier fluid, a standard delivery method for respiratory studies in mice (Helms *et al.*, 2010). Using this method it was only possible to deliver small quantities of particulates (typically 1% *w/v*) because larger concentrations fell out of suspension extremely rapidly. It is also likely that the accompanying carrier fluid perturbed the airway surface and altered both the manner of deposition and the post-deposition MCT behaviour being measured. Furthermore, instillation tends to target the distal regions of the lung and parenchyma compared with the upper respiratory tract where

most particulate deposition naturally occurs (Helms *et al.*, 2010).

The aim of this study was to verify that synchrotron PCXI could be used to detect, monitor and compare the deposition and transit behaviour of individual and groups of pollutant particles after *dry deposition* into the trachea of live mice, to better mimic environmental pollutant particle exposure. Using a dry powder insufflator, and commonly inhaled pollutants, we sought to document particle and fibre visibility and post-deposition MCT behaviour on the *tracheal* airway surface. We also aimed to determine whether the dry delivery method resulted in different post-deposition behaviour compared with the saline carrier method used previously (Donnelley *et al.*, 2009; Donnelley, Siu *et al.*, 2010).

## 2. Methods

Experiments were performed on the BL20XU undulator beamline at the SPring-8 synchrotron radiation facility in Japan, under approval from the Animal Ethics Committee of SPring-8 and of the Women's and Children's Health Network, Adelaide.

### 2.1. Imaging set-up

The experimental hutch was located in the Biomedical Imaging Centre, 245 m from the storage ring, and the imaging layout was as used previously (Parsons *et al.*, 2008). Monochromatic 25 keV ( $\lambda = 0.5 \text{ \AA}$ ) X-rays were selected using a standard double-crystal monochromator (Yabashi *et al.*, 1999). At the imaging station the beam size was approximately 4 mm (H)  $\times$  2 mm (V). A propagation (sample-to-detector) distance of  $\sim 95$  cm was chosen to produce a sufficiently strong bright/dark fringe from the boundary of each particle, so that they could be detected amid intensity variations introduced by overlying tissue and skin. Images were captured using a high-resolution X-ray converter (AA50 Hamamatsu Photonics) with a charge-coupled device (CCD) detector. The converter used a 10  $\mu\text{m}$ -thick scintillator ( $\text{Lu}_2\text{SiO}_5:\text{Ce}$ ) to convert X-rays to visible light, which was then directed to the CCD using a 20 $\times$  microscope objective lens (NA 0.4). The CCD detector was a pco.4000 (PCO Imaging) with an array size of 4008  $\times$  2672 pixels and a 9  $\mu\text{m}$   $\times$  9  $\mu\text{m}$  native pixel size. This set-up resulted in an effective isotropic pixel size of 0.45  $\mu\text{m}$  and a field of view of 1.8 mm  $\times$  1.2 mm. The incident beam was limited to this size using slits to reduce the radiation dose to the animals. The FWHM of the point spread function, as determined from an image of a highly attenuating horizontal edge, was 3.6  $\mu\text{m}$ . Image capture was synchronized with a fast shutter (Uniblitz XRS6 with VMM-T1 timer unit) and triggered by the ventilator (refer to the animal preparation description below) to minimize the dose between exposures. An exposure time of 50 to 80 ms was optimal for capturing sufficient X-ray photons to fill the potential dynamic range ( $2^{14}$  grey levels) of the detector, providing the maximal signal-to-noise ratio without inducing detector saturation.

## 2.2. Sample preparation

In this experiment four of the particle samples previously tested in the mouse nasal (Donnelley *et al.*, 2009) and tracheal airways (Donnelley, Siu *et al.*, 2010) were utilized. Fibreglass from a commercial pipe insulation and lead sulfide (PbS), present in lead-ore and the primarily component of dust produced during lead smelting (Spear *et al.*, 1998), were both finely ground using a mortar and pestle. Dolomite quarry dust that settled out of airborne suspension was provided courtesy of the Boral Resources (SA) Limited Linwood Quarry (Adelaide, South Australia). Hollow silver-coated glass beads with a median diameter of 14  $\mu\text{m}$  were obtained from Potter Industries (Melbourne, Australia) for use as high-visibility reference particles of known composition, shape and size. Asbestos was not tested in this experiment as the preparation of *dry* asbestos fibres in the imaging hutch was deemed an unacceptable occupational health and safety hazard. The size distribution of the samples was determined in a previous study and typically ranged from 5  $\mu\text{m}$  up to 12  $\mu\text{m}$  diameter with a small number of larger particles present [see Fig. 3 in Donnelley, Siu *et al.* (2010)].

## 2.3. Animal preparation

The experiment was performed using eight C57Bl/6 mice weighing  $\sim 18$ – $20$  g. Animal preparation was based on methods described previously (Donnelley, Parsons *et al.*, 2010). Mice were anaesthetized with pentobarbital (Somnopenil, Pitman-Moore, Washington Crossing, USA, 100 mg  $\text{kg}^{-1}$  i.p.). The imaging area around the trachea was cleared of fur using depilatory cream (Nair, Church & Dwight, Australia). The mice were intubated using a fibre-optic illuminated guide wire and a 20 Ga i.v. catheter (Insyte, Becton Dickinson, Utah, USA) as an endotracheal (ET) tube (Hamacher *et al.*, 2008). The ET tube was inserted into the trachea to a fixed depth of 22.5 mm from the nose tip, placing the ET tube tip approximately half way between the epiglottis and the carina, thus avoiding physical perturbation of the more distal imaging region. The catheter needle-hub was immediately cut off to minimize respiratory dead-space and so that the ET tube was ready for connection to the ventilator. Mice were secured to a polyethylene imaging board with their dorsal incisors hooked over a stainless-steel wire loop and the limbs, shoulders and torso taped to the board to minimize body movements that interfere with high-resolution imaging.

The imaging board was mounted on the hutch sample stage such that the mouse was oriented supine and the X-ray beam passed laterally through the mouse trachea, at approximately five cartilage rings below the tip of the ET tube. During the experiment anaesthesia was maintained by constant infusion of pentobarbital (0.1 mg  $\text{kg}^{-1}$   $\text{s}^{-1}$  *via* an indwelling i.p. needle) from a syringe pump (UltraMicroPump III and Micro4 controller, World Precision Instruments, Florida, USA). The ET tube was attached to a flexiVent small animal ventilator (SCIREQ, Canada) connected to 100%  $\text{O}_2$  *via* a HC100 respiratory humidifier (Fisher and Paykel, Auckland, New Zealand). Ventilation was set at 80 breaths  $\text{min}^{-1}$ , a tidal

volume of 20 ml  $\text{kg}^{-1}$  (minute ventilation of approximately 1.6 ml  $\text{g}^{-1}$ ) and  $\sim 3$  cm  $\text{H}_2\text{O}$  of PEEP. The ventilatory profile was configured with  $T_{\text{inspiration}} = 0.2$  s,  $T_{\text{pause}} = 0.15$  s and  $T_{\text{expiration}} = 0.4$  s (inspiratory-to-expiratory ratio of 87.5%). The flexiVent provided a trigger to capture a single image during each end-inspiratory pause. Body temperature was maintained using an infrared heat lamp and monitored with a rectal thermometer, and vital signs were monitored using a MouseOx pulse oximeter (STARR Lifesciences, USA).

## 2.4. Sample delivery

Owing to the small number of available animals and limited synchrotron beam time, all mice first received hollow silver-coated glass beads ( $n = 8$ ). Six of the mice then also received one of the remaining three particulates ( $n = 2$  per particulate).

After 30 s of baseline collection (40 images) a DP-4 dry powder insufflator and AP-1 air pump (PennCentury, Wyndmoor, PA, USA) were used to deliver a sample of the hollow glass beads into the trachea and conducting airways *via* the ET tube. Owing to high variability in the output (mass) of the first actuation of the air pump, the first output was discarded and the second actuation was used to deliver the sample to the airways. The insufflator was weighed using a fine balance before the second actuation and after sample delivery to verify the mass delivered to the mouse airways. Basing our delivered doses on mass rather than volume proved to be a precise way of ensuring that the quantity of each delivered sample was reliably precise and repeatable. The insufflator was thoroughly cleaned with compressed air between deliveries to remove any residual particles. After glass beads were delivered, the same process was used to deliver the second particulate.

To deliver a particulate sample to the mouse airway the hutch door was opened, the ET tube manually disconnected from the flexiVent, the sample delivered *via* the ET tube, the flexiVent reconnected and the hutch door closed. Typically there was a delay of 1 min between sample delivery and imaging. Image acquisition continued for a further 5 min (400 images). A second instillation of particles, *i.e.* lead, fibreglass or quarry dust, followed by imaging, created a dataset consisting of 840 images per mouse.

## 2.5. Post-experimental analyses

After completion of each experiment, mice were humanely killed *via* overdose of pentobarbital (500 mg  $\text{kg}^{-1}$  i.p.), without loss of anaesthesia. All image sequences were flat-field and dark-current corrected (Matlab R2010a, The Mathworks, Natick, MA, USA). For high-quality motion-detection the background must remain still compared with the moving objects, hence special efforts were made to minimize the movement of the mouse during imaging, including the use of restraining boards and respiratory-gating as described. Where appropriate, specific details of the image analyses are given in the figure legends.

Although it was not the primary goal of the experiment,  $\sim 50$  selected individual non-stationary particles were manually tracked throughout the image sequences to estimate the

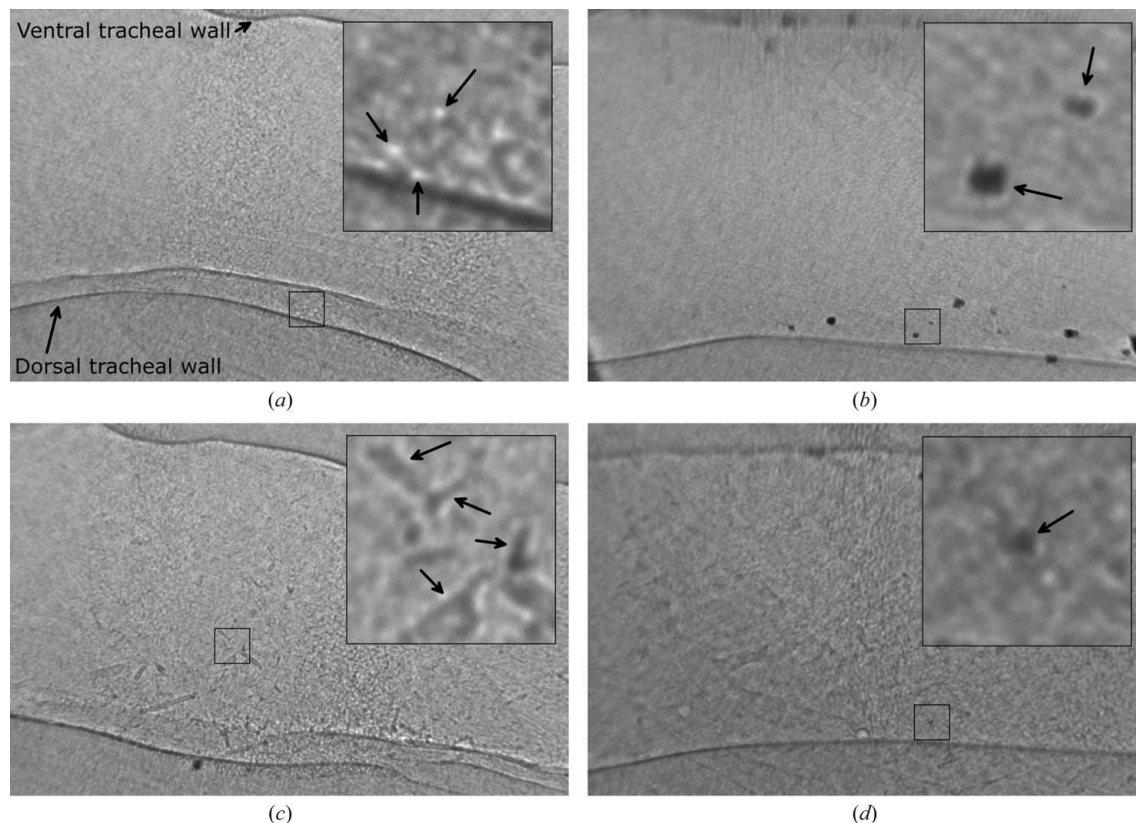


**Figure 1**

All four pollutant and marker particles were visible on the tracheal airway surface. These static frames (taken from each of the four supplementary movies) show (a) glass beads, (b) lead, (c) fibreglass and (d) quarry dust. Each image contains an inset showing a small segment of the airway surface at higher magnification to aid identification of the particulates. Each image is 1.8 mm × 1.2 mm (insets are ~0.1 mm × 0.1 mm). The head is to the right and lungs are to the left, with MCT expected to be predominantly in the left-to-right direction. Note the presence of cartilage bands [broad speckled regions in (a), (b) and (d)] surrounding the trachea, and the glass beads remaining in (d) from the first delivery.

average MCT rate (mean ± standard deviation) of each particle type when moving. This analysis only measured the distance particles travelled over time and did not take into account the pattern of their transit behaviour.

Supplementary movie files were assembled from the post-deposition images and show particulate and fibre behaviour on the tracheal airway surface.<sup>1</sup> Each video shows five minutes of airway surface activity and consists of 400 frames (one frame acquired per breath). The movie frame rate is set to 7.5× normal speed. All videos are avi files, were encoded using the *Xvid* codec and can be played using the free VLC Media Player (available at <http://www.videolan.org/vlc/>).

### 3. Results

Using the dry powder insufflator ~0.1 mg of each particulate material was delivered to the airways. This corresponded to a ~600× greater mass of particulates compared with our previous study (Donnelley, Siu *et al.*, 2010). Each particulate type was immediately visible in the PCXI images, but the majority were stationary when observation began. Fibreglass

and lead were the most clearly visible particles, but glass beads and a small number of quarry dust particles could also be detected, particularly once they began to transit the airway surface. The appearance of the four tested particle types is shown in Fig. 1. Despite thorough cleaning of the insufflator between each delivery (performed according to the manufacturer's directions), minor cross-contamination was sometimes visible; for example, a single dark lead particle is present in the fibreglass study (Fig. 1c).

This distance between the X-ray source and the sample on this beamline is 245 m, so any instabilities in the source (*e.g.* electron orbit, optics vibrations owing to thermal or vacuum instabilities and so on) are exacerbated by a lever arm effect. This noticeably affected the quality of the acquired images, particularly the upper (ventral) portion of the trachea. This is evident in Figs. 1(b) and 1(d) and in the supplementary movies (a band of rapid intensity fluctuations or flickering, particularly across the top of the image) where the upper tracheal edge and nearby particles are blurred compared with the same features on the bottom (dorsal) surface. The exposure length was also chosen to be sufficiently short so as to ensure that image blurring did not occur; however, we suspect that in some cases motion of the airway (caused by movement during the iso-pressure breath hold) did result in some blurring, again particularly at the ventral tracheal surface.

<sup>1</sup> Supplementary data for this paper are available from the IUCr electronic archives (Reference: MO5033). Services for accessing these data are described at the back of the journal.

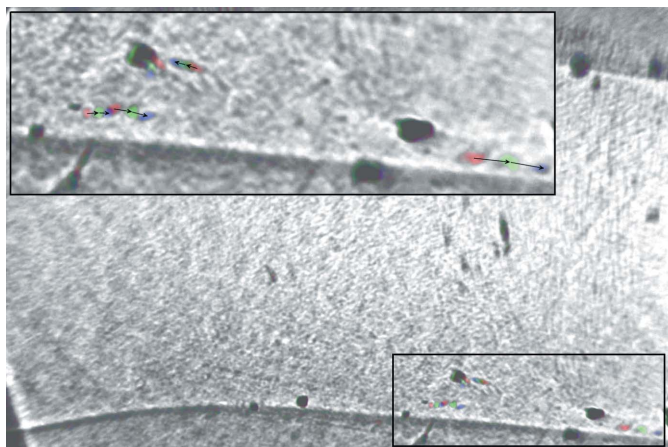


**Figure 2**

Artificially coloured image showing the movement of lead particles on the airway surface. Three consecutive frames were taken and the intensity colour map modified for each such that black (*i.e.* lowest intensity) was replaced by red (frame 1), blue (frame 2) and green (frame 3), rendering the highly attenuating lead particles in each of these colours. The three frames were then added, so that moving particles could be seen in colour, with stationary particles seen in black (the sum of red, green and blue). In the inset the dorsal edge of the trachea is magnified  $2\times$  and particles can be seen moving at different rates and in different directions (as marked) along the airway surface. The small colour changes surrounding the large particles represent minor fluctuations from airway movement. As in Fig. 1 the head is to the right and the lungs are to the left. The main image is  $1.8\text{ mm} \times 1.2\text{ mm}$  (inset is  $\sim 0.72\text{ mm} \times 0.24\text{ mm}$ ).

The first movement of the particulates in the field of view appeared two to three minutes after delivery. As in previous studies the particle transit was heterogeneous: after deposition some particles did not move while others transited the field of view rapidly. In most cases the larger particles moved substantially less than the smaller particulates. In addition, many particles did not follow a linear MCT path along the airway: they followed what appeared to be random circling paths. In general, particle movement was concentrated along the dorsal quarter of the tracheal surface. Fig. 2 shows an example of the movement of lead particles along the dorsal tracheal surface; artificial colouring reveals the different rates and different directions of particle movement. In some animals radial and axial contraction of the tracheal airway was also observed within the imaging period (*e.g.* Fig. 1*a*). None of the fibreglass fibres moved after deposition. In contrast, the glass bead MCT rate was approximately  $1.28 \pm 0.8\text{ mm min}^{-1}$ , lead was  $1.82 \pm 1.6\text{ mm min}^{-1}$  and quarry dust was  $1.74 \pm 0.8\text{ mm min}^{-1}$ .

### 3.1. Supplementary movie descriptions

The dynamics of airway surface MCT are difficult to adequately describe or to show in static images, so the four supplementary movies provided with this paper should be viewed to best appreciate the nature of particle movement. These movies demonstrate that particle and fibre visibility is dramatically enhanced in *dynamic* sequences when compared with the *static* images presented in Fig. 1. The chosen

supplementary movies are representative of the movies created for each particle type.

There are several details to consider when viewing the images. Firstly, it is important to note that in these X-ray images (the static images and movie sequences) particle activity on both (lateral) tracheal walls is superimposed, so it is not possible to determine which surface (*i.e.* near or far) the particulates are located on. Secondly, some particulates and particulate motion appears to be located below the apparent tracheal edge (Figs. 1*a* and 1*c*). This phenomenon is due to the  $\omega$ -shaped dorsal wall of the trachea formed by an epithelial protrusion in the dorsal surface of the trachea overlying the trachealis muscles, *i.e.* the dorsal trachea has a characteristic centrally flattened  $\omega$  shape. Thirdly, in all supplementary movies some remnants of individual fur shafts are also visible despite depilation and can be identified as moving with the overlying skin artefacts.

**3.1.1. Supplementary movie 1: hollow glass beads.** No bead movement is visible until approximately frame 40 (30 s after imaging starts and approximately 90 s after sample delivery) when the first wavefront of massed beads appears moving toward the mouth (to the right) and extending to approximately 20% of the tracheal height. The rate of bead movement varies with time and location along the trachea. At frame 114 the sample stage was moved so that the bottom edge of the trachea remained within the field of view.

Note that although ‘cilial-like’ activity is present, the magnification of structures within these images is orders of magnitude lower than that required to resolve individual cilia. We speculate that this optical effect is speckle caused by refraction of the X-rays through large numbers of small beads aggregating along the dorsal wall of the trachea as they are propelled by the underlying massed ciliary actions (Kitchen *et al.*, 2004).

The entry and movement of beads reveals regions of ciliary transit patterns, both individual and bulk, that would otherwise not be apparent. Retrograde, stationary, linear, circular and stop–start patterns of behaviour are all visible (this effect is also present for lead particles; see supplementary video 2). A small number of contaminant lead particles are also visible flowing in linear and/or circular patterns before stopping.

**3.1.2. Supplementary movie 2: lead.** Three distinct patterns of airway surface activity appear to be associated with the lead particles. Some particles are immobile. On the dorsal surface a minority of the lead particulates are transported directly along the trachea towards the head (*i.e.* to the right). The remainder (typically  $\sim 15\text{ }\mu\text{m}$  diameter) appear trapped in an eddy-like MCT pattern near a substantially larger particle ( $\sim 140\text{ }\mu\text{m}$ , measured at frame 330). Although less distinct, the movement of ventral (*i.e.* located toward the top of the image) particles is directed obliquely towards the dorsal surface (*i.e.* the bottom of the image), with most particles in this case eventually trapped and left immobile approximately half way down.

**3.1.3. Supplementary movie 3: quarry dust.** By comparison with the other supplementary movies [and Figs. 1(*a*)–1(*c*)] only small numbers of quarry dust particles can be seen and they are less distinct than glass bead or lead particles. Residual

glass beads from the first delivery are also apparent along the left-hand edge of the image moving slowly ventrally then retrograde (*i.e.* towards the lung) in the first half of the sequence. Some immobile contaminant dark lead particles are present along the ventral (upper) tracheal edge. Several quarry dust particles begin their transit along the dorsal tracheal edge from the left-hand side at the start of the movie. In this image series some dust particles leave the dorsal surface (starting at a point approximately three-quarters across the frame) and follow a more ventral MCT path. Towards the end of the sequence other dust particles can be seen following rotating MCT paths above the dorsal tracheal surface (approximately half way across the frame). Some quarry dust particles transit the airway surface and then disappear.

**3.1.4. Supplementary movie 4: fibreglass.** Fibres are immediately obvious, distributed in random orientations, predominantly along the dorsal (bottom) half of the trachea. A comparison of the initial and final frames showed that in contrast to the other particle types all the fibres were essentially immobile within the trachea over the imaging period, regardless of their size. Although the fibres did not move, some residual bead movement (from the first insufflation) can be seen occurring along the dorsal wall until approximately frame 100.

The mouse was moved (*via* a motorized sample stage) three times while images were being captured (at frames 17, 26 and 34) to ensure the bottom edge of the trachea remained within the field of view. Dorsal folds of trachea, apparent as additional white edges near the bottom of the trachea, are present centrally and on the right-hand side of the frame [see Figs. 1(a) and 1(c)]. Again, an unexpected single large lead particle is present and can be seen rapidly transiting the dorsal wall before slowing and halting approximately two-thirds across the frame.

## 4. Discussion

The primary finding of this study is that the use of dry particle insufflation greatly improves the ability to detect and to track particle MCT along live mouse airways using PCXI. Both pollutant-particle and marker-particle transit was clearly revealed following dry deposition. Particle transit was more clearly visible in the *dynamic* video sequences than the *static* images owing to the phenomenon of ‘motion popout’ whereby moving objects are identified by retinal motion (Abrams & Christ, 2003; Rushton *et al.*, 2007). This means that very small particulates (<5 µm) could be detected provided they were moving, but were essentially invisible when stationary.

The main strength of this approach is that particulates are delivered in a more physiologically realistic manner than in previous experiments. In comparison with our earlier tracheal deposition studies using a saline carrier fluid (Donnelley, Siu *et al.*, 2010), dry insufflations allowed us to deliver a greater number of particles and fibres into the trachea, greatly improving our ability to visualize and describe the MCT patterns that were present. We expect that most dry particles

are initially deposited on the moist tracheal and conducting airway surface liquid rather than being washed deeper down into the conducting airways and lung parenchyma. More importantly, independent of the increased number of particles, particle motion was more clearly visible after dry deposition than after fluid-carrier deliveries (Donnelley, Siu *et al.*, 2010). We speculate that this might be because dry particles are not submerged in the carrier fluid and therefore produce stronger phase-contrast effects on the airway surface, enhancing their visibility.

The calculated average particle MCT rates (between 1.3 and 1.8 mm min<sup>-1</sup>) were greater than after fluid-carrier particle delivery [ $\sim 0.37$  mm min<sup>-1</sup> for glass beads, as reported by Donnelley, Siu *et al.* (2010)]. We propose that in the fluid-carrier experiment the addition of the fluid to the airway surface may have inhibited effective particle MCT during the imaging period, resulting in slower particle transit rates. Grubb *et al.* (2004) determined that bulk mouse tracheal MCT was 2.2 mm min<sup>-1</sup> using a dye transit technique, indicating our findings are consistent with the existing literature, and suggesting that dry particle delivery can provide more accurate measurement of the particle MCT rate under synchrotron PCXI imaging.

The pattern of MCT observed for each particle type was often different. The appearance of a ‘wavefront’ of small glass beads that moved along the trachea was not observed for the other particles. Since the glass beads are hollow they are readily discernible using PCXI (which enhances boundaries), and it may be that the large number of delivered small beads underlies this particular difference. Regardless, our findings suggest that hollow glass beads may be a valuable marker particle for revealing local MCT patterns and for estimating the local individual and bulk motions of particles being transported by MCT processes. The glass bead marker particle behaviour highlights that MCT is not a uniform process as suggested by radiolabel studies (Grubb *et al.*, 2004), and this technique may therefore have potential for discovering mechanisms of toxic pollutant particle and fibre retention, in addition to their effect on airway health. The frequent presence of rotating ‘eddy-like’ areas of MCT in intact live airways that are visible in the supplementary movies could not be revealed *in vivo* without the use of these particulates to visualize the nature of the airway surface activity.

Although we observe particle movement during this short period, the particulates are by no means completely cleared from the airways. In many cases particles stopped moving, but the mechanisms controlling that change in motion cannot be determined by these studies. Some particles remain in place, and we interpret these as being held immobile by the surface mucus forces. However, the function of the MCT mechanisms is to *clear* particles, so we speculate that if the imaging period extended over hours then these immobile particles would normally be eventually cleared, whether by MCT or by cough mechanisms. We also speculate that the clearance of fibres may take substantially longer than the dust particles. Clearance is a two-phase process, with a fast clearance phase that results in the bulk of the particles being cleared within 24 h,

and a slow clearance phase that removes additional particles over a period of multiple days (Falk *et al.*, 1999; Hofmann & Asgharian, 2003; Möller *et al.*, 2004). Other studies have demonstrated the effect of small pollutant particles on lung tissue several days after exposure (Tong *et al.*, 2006; Zhang *et al.*, 2007), but little is known about the long-term *in vivo* behaviour of deposited particles. In future experiments we plan to examine particle MCT over a period of days using a repeated-measures study design.

The prevalence of particles found near the dorsal wall after dry insufflation may be due to the supine positioning of the mice (*i.e.* a gravitational effect). Since all fibreglass fibres were immobile immediately after deposition, the distribution of fibres towards the dorsal surface suggests that either gravity or the particle delivery method may influence the deposition location. However, in the carrier fluid study most glass beads were also detected close to the dorsal tracheal wall. In that study the mice were mounted head-high on the hutch sample stage, indicating that gravity was unlikely to have played a significant role in that study. This supports the notion that although gravity may assist deposition along the dorsal surface it is not the only influence. Indeed, that common movement of particles from the ventral to the dorsal regions of the trachea (see supplementary movie 2) indicates that MCT patterns drive particles towards the dorsal surface. In future studies we plan to examine the effects of gravity on particle deposition patterns and post-deposition MCT behaviour.

The sizes of lead particles detected in the trachea in this dry deposition study were different from the distribution observed in the carrier fluid study, despite the samples being drawn from the same batch of material. We speculate that the density of the heavy (larger) lead particles caused a rapid settling within the carrier fluid and prevented them from being drawn up in the fluid-delivery bolus. Alternatively, if large lead particles were present in the bolus they were not expelled to the region of the airway that we imaged. Although our sample size was small we also did not see clusters of lead particles similar to those visible in the carrier fluid studies [galena supplementary video (Donnelley, Siu *et al.*, 2010)].

Substantially more fibreglass was visible after dry insufflation, but as in the carrier fluid study the visible dry-deposited fibres were immobile throughout the imaging period. We can only speculate that the fibres may bridge many cilia so that no net movement can occur, or there is another physical (such as their long needle-like shape) or chemical property that causes the fibres to lodge on the airway surface more securely than for the other particles, possibly increasing their toxicity compared with generally circular particulates (*i.e.* dusts). The inability to effectively clear fibres from the airway might influence airway health and warrants further investigation.

Considering that the same mass of each sample was delivered, we were surprised by the small number of quarry dust particles present. A proportion of the quarry dust is soluble, so one explanation is that some dust dissolved after contacting the wet airway surface, leaving only the insoluble particles remaining. Fig. 2(b) in our previous study (Donnelley, Siu *et al.*, 2010) shows that quarry dust is generally less visible than

the other particulates tested, so it is also likely that it is more difficult to detect in the trachea of live mice. In addition, because the human visual system excels at detecting moving particles, it is also possible that the quarry dust was not visible because many of the dust particles did not move substantially after deposition, also explaining why those dust particles that stopped moving seemed to ‘disappear’ from view.

Limitations of this study include the reduced image quality caused by X-ray beam instability and the movement during image capture caused by the inability of the flexiVent isopressure breath hold to maintain a completely still trachea. In future experiments an end-expiratory pause may be combined with a drug that produces respiratory muscle paralysis to minimize movement artefacts. Although the frame rate was higher (1.2 Hz) than for our previous studies ( $\sim 0.1$  Hz), it may still be too low for optimal particle imaging when taking into account the magnification and MCT rate of some particles. With new camera technology we expect that this will improve in the future. The number of particles visible also varied despite delivering similar weights to each animal, and attention to delivering more comparable amounts (*e.g.* measuring samples by volume rather than weight) is needed to improve comparability. It is likely that, because the delivered quantities are minute and each particulate sample type has different physicochemical properties (including density, median diameter, static electricity effects, *etc.*), they can behave differently during insufflation. Finally, despite thorough cleaning of the insufflator some contaminant particulates were visible in most image sequences. However, these did not influence the study outcomes because the contaminants could be clearly identified.

In summary, this study verified that synchrotron PCXI is a powerful tool for examining the post-deposition MCT behaviour of commonly inhaled pollutants after deposition into the airways of live mice using a dry powder insufflator. The use of a dry delivery system resulted in a greater number of delivered particles, improved particle visibility and different post-deposition behaviour than when delivering particles suspended in a carrier fluid. We propose that the dry delivery system is also a more physiologically realistic method of particle delivery, producing particle MCT rates more consistent with the existing literature than our previous wet-delivery studies. We are continuing with studies to improve our direct and non-invasive MCT assessment methods to assist our understanding and treatment of respiratory diseases such as CF.

These studies were supported by the NH&MRC Australia and philanthropic donors *via* the CURE4CF Foundation (<http://www.cure4cf.org/>). The synchrotron radiation experiments were performed on the BL20XU beamline at SPring-8, with the approval of the Japan Synchrotron Radiation Institute (JASRI) under proposal number 2010B1137. Dr Andreas Fouras, Monash University Division of Biological Engineering, provided imaging advice and supplied essential experimental equipment including the CCD detector. Mr Paul Whiffen, Environment Manager, Boral Resources (SA)

Limited, provided dolomite quarry dust samples. KSM was supported by an Australian Postgraduate Award, a Monash University J. L. William Scholarship and a Cystic Fibrosis Australia Studentship. MD, KSM, KKWS and DWP were supported by the Australian Synchrotron International Synchrotron Access Program. The ISAP is an initiative of the Australian Government being conducted as part of the National Collaborative Research Infrastructure Strategy.

### References

- Abrams, R. A. & Christ, S. E. (2003). *Psychol. Sci.* **14**, 427–432.
- Cloetens, P., Barrett, R., Baruchel, J., Guigay, J. P. & Schlenker, M. (1996). *J. Phys. D.* **29**, 133–146.
- Donaldson, S. H., Corcoran, T. E., Laube, B. L. & Bennett, W. D. (2007). *Proc. Am. Thorac. Soc.* **4**, 399–405.
- Donnelley, M., Morgan, K. S., Fouras, A., Skinner, W., Uesugi, K., Yagi, N., Siu, K. K. W. & Parsons, D. W. (2009). *J. Synchrotron Rad.* **16**, 553–561.
- Donnelley, M., Parsons, D., Morgan, K. & Siu, K. (2010). *AIP Conf. Proc.* **1266**, 30–34.
- Donnelley, M., Siu, K., Jamison, A. & Parsons, D. (2011). *Gene Ther.* **19**, 8–14.
- Donnelley, M., Siu, K. K. W., Morgan, K. S., Skinner, W., Suzuki, Y., Takeuchi, A., Uesugi, K., Yagi, N. & Parsons, D. W. (2010). *J. Synchrotron Rad.* **17**, 719–729.
- Falk, R., Philipson, K., Svartengren, M., Bergmann, R., Hofmann, W., Jarvis, N., Bailey, M. & Camner, P. (1999). *Exp. Lung Res.* **25**, 495–516.
- Goss, C. H., Newsom, S. A., Schildcrout, J. S., Sheppard, L. & Kaufman, J. D. (2004). *Am. J. Respir. Crit. Care Med.* **169**, 816–821.
- Grubb, B. R., Jones, J. H. & Boucher, R. C. (2004). *Am. J. Physiol. Lung Cell. Mol. Physiol.* **286**, L588–L595.
- Hamacher, J., Arras, M., Bootz, F., Weiss, M., Schramm, R. & Moehrlen, U. (2008). *Lab. Anim.* **42**, 222–230.
- Happo, M. S., Salonen, R. O., Hälinen, A. I., Jalava, P. I., Pennanen, A. S., Dormans, J. A., Gerlofs-Nijland, M. E., Cassee, F. R., Kosma, V. M., Sillanpää, M., Hillamo, R. & Hirvonen, M. R. (2010). *Inhal. Toxicol.* **22**, 402–416.
- Helms, M. N., Torres-Gonzalez, E., Goodson, P. & Rojas, M. (2010). *J. Vis. Exp.* **42**, e1941 (doi:10.3791/1941).
- Hofmann, W. & Asgharian, B. (2003). *Toxicol. Sci.* **73**, 448–456.
- Hua, X., Zeman, K. L., Zhou, B., Hua, Q., Senior, B. A., Tilley, S. L. & Bennett, W. D. (2010). *J. Appl. Physiol.* **108**, 189–196.
- Kitchen, M. J., Paganin, D., Lewis, R. A., Yagi, N., Uesugi, K. & Mudie, S. T. (2004). *Phys. Med. Biol.* **49**, 4335–4348.
- Limberis, M., Anson, D. S., Fuller, M. & Parsons, D. W. (2002). *Hum. Gene Ther.* **13**, 2112.
- Livraghi, A. & Randell, S. H. (2007). *Toxicol. Pathol.* **35**, 116–129.
- Möller, W., Häussinger, K., Winkler-Heil, R., Stahlhofen, W., Meyer, T., Hofmann, W. & Heyder, J. (2004). *J. Appl. Physiol.* **97**, 2200–2206.
- O'Connor, G. T., Neas, L., Vaughn, B., Kattan, M., Mitchell, H., Crain, E. F., Evans, R., Gruchalla, R., Morgan, W., Stout, J., Adams, G. K. & Lippmann, M. (2008). *J. Allergy Clin. Immunol.* **121**, 1133–1139.e1.
- Parsons, D. W., Morgan, K., Donnelley, M., Fouras, A., Crosbie, J., Williams, I., Boucher, R. C., Uesugi, K., Yagi, N. & Siu, K. K. (2008). *J. Anat.* **213**, 217–227.
- Rushton, S. K., Bradshaw, M. F. & Warren, P. A. (2007). *Cognition*, **105**, 237–245.
- Siu, K. K., Morgan, K. S., Paganin, D. M., Boucher, R., Uesugi, K., Yagi, N. & Parsons, D. W. (2008). *Eur. J. Radiol.* **68**, S22–S26.
- Snigirev, A., Snigireva, I., Kohn, V., Kuznetsov, S. & Schelokov, I. (1995). *Rev. Sci. Instrum.* **66**, 5486–5492.
- Spear, T. M., Svee, W., Vincent, J. H. & Stanisich, N. (1998). *Environ. Health Persp.* **106**, 565–571.
- Stocker, A., Kremer, K., Koldej, R., Miller, D., Anson, D. & Parsons, D. (2009). *J. Gene Med.* **11**, 861–867.
- Tong, Y., Zhang, G., Li, Y., Tan, M., Wang, W., Chen, J., Hwu, Y., Hsu, P. C., Je, J. H., Margaritondo, G., Song, W., Jiang, R. & Jiang, Z. (2006). *Eur. J. Radiol.* **58**, 266–272.
- Wilkins, S. W., Gureyev, T. E., Gao, D., Pogany, A. & Stevenson, A. W. (1996). *Nature (London)*, **384**, 335–338.
- Yabashi, M., Yamazaki, H., Tamasaku, K., Goto, S., Takeshita, K., Mochizuki, T., Yoneda, Y., Furukawa, Y. & Ishikawa, T. (1999). *Proc. SPIE*, **3773**, 2–13.
- Zhang, G. L., Yue, W. S., Liu, P., Sun, J. Q., Hwu, Y. K., Je, J. H., Tan, M. G. & Li, Y. (2007). *Nucl. Instrum. Methods Phys. Res. B*, **262**, 304–312.